Penetration and Fracture of Sea Ice Due to Impact Loading

Bernard Ross

Stanford Research Institute, Menlo Park, California, U.S.A.

Abstract

Impact tests were made on floating ice slabs with particular attention devoted to the mechanism of penetration*. The range of values investigated for the basic parameters was: impact velocity, 8~21 ft/sec; projectile mass, 4.56~5.22 lb, and penetrator diameter, $^5/_{16}$~$1^1/_4$ in. The perforation of ice slabs made from seawater, and at approximately +17°F (warm sea ice), was obtained by the ejection of a shear plug from the test slab, whereas fresh-water ice slabs under similar loading conditions fractured into segments along well defined radial cleavage planes. The experiments indicated that a blunt end penetrator profile was significantly more effective in the perforation of warm sea ice than a penetrator with conical profile. In addition, the order of magnitude of the impact velocity and temperature of the ice slab were important factors that governed the mechanism of penetration.

For shear plug ejection, a simple mathematical model based upon the laws of conservation of linear momentum and mechanical energy provides correlation between impact energy and a quantity containing penetrator diameter and sea ice thickness. Using these quantities, curves can be presented which indicate a threshold-of-perforation boundary for the warm sea ice.

Finally, an appendix is included which summarizes the most recent work in this problem and gives results obtained since the writing of the original paper. A new sea ice manufacturing scheme produces test slabs of significantly lower salinity contents. These slabs evidence a different mechanism of perforation resulting in "cylindrical-conical" shear plugs. A mathematical theory incorporating this model is presented and its predictions compared with results obtained from tests on styroform and sea ice slabs. Agreement is good within the range of variables explored.

Symbols

c	location of projectile center of gravity
D	diameter of penetrator
g	acceleration due to gravity
h	height above ice slab at which the projectile mass is released
m_1	mass of the projectile and penetrator
m_2	mass of the ejected shear plug
t	thickness of ice slab
v_1	velocity of projectile immediately prior to impact
v_2	velocity of projectile and shear plug immediately after impact
x, y	coordinate directions, see Fig. 9
η	running coordinate, see Fig. 9
$\tau_{xy}(\eta, \dot{\eta})$	shear yield stress function
τ_{xy_0}	constant value of shear yield stress acting on plug during ejection, see Fig. 9

* Possible mechanisms of perforation are shown in Fig. 1.

I. Introduction

The possibility of air-dropping scientific instrumentation packages in remote ice covered regions of the Arctic to explore phenomena characteristic of the underlying ocean has initiated studies concerned with the penetration behavior of sea ice subjected to impact loading. Although abundant literature exists concerning research in ice and snow physics as well as engineering problems posed by the arctic environment (Kingery, 1963; Wilson, 1964), and even though the penetration of frozen ground by piles and projectiles has been investigated in the past (Benert, 1963; Charest *et al.*, 1965), it appears that little or no previous attention has been given to the mechanics of sea ice penetration and, in particular, the penetration of floating ice slabs. Therefore, the present study was undertaken as the initial phase of an experimental and analytical program designed to provide knowledge in this subject.

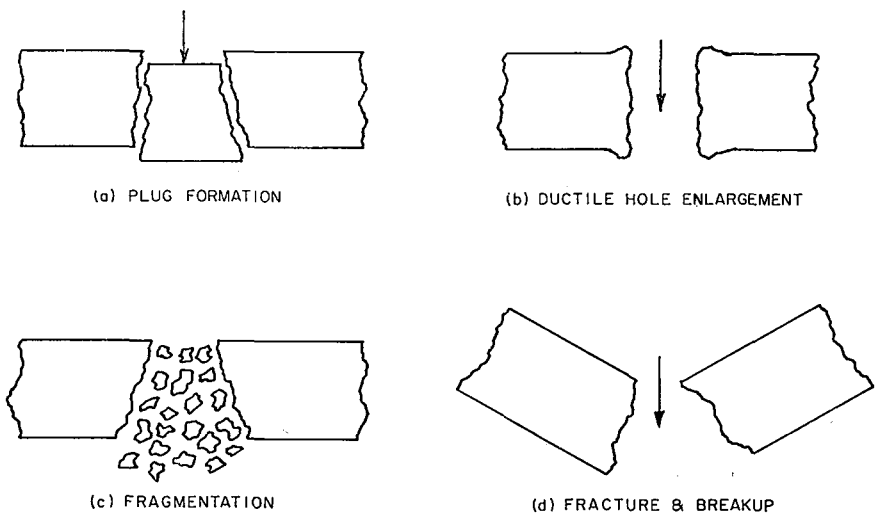

Fig. 1. Possible mechanisms for ice slab perforation

The problem can be posed simply. Given: A projectile of specified shape, dimensions and weight which is released with known initial velocity from a particular height. Required: A measure of probability that the projectile will perforate (completely penetrate) the ice cover and, therefore, be able to fulfill its objectives underwater.

II. Test Specimens, Equipment and Procedure

A series of sea ice test specimens manufactured from Pacific Ocean water was employed in the investigation. In addition, a limited number of tests were performed on freshwater ice. All tests specimens were circular slabs having a diameter of 28 in. and a thickness at the start of the experiment of $3\frac{1}{2}$ to 4 in. A representative example of the test slabs can be seen in Fig. 2.

All of the numerical data were acquired for sea ice slabs at approximately $17\pm1°F$ (warm sea ice). However, a few tests that provided only qualitative data were carried

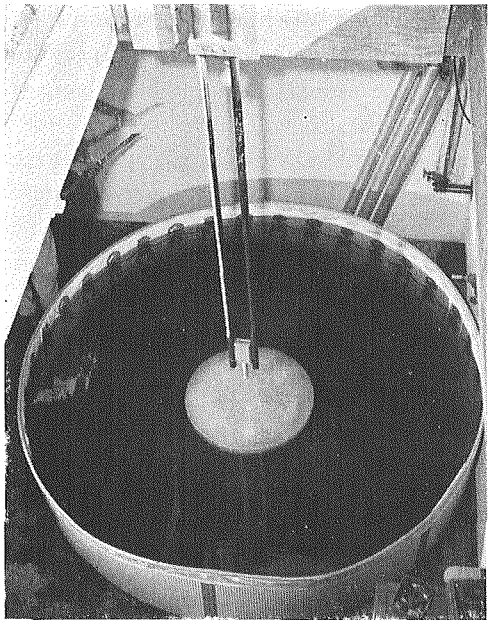

Fig. 2. Test facility

out on a subzero sea ice slab having a thickness of $4^3/_4$ in. and an average slab temperature of −13°F.

A typical test specimen was manufactured over a 72-hour period by freezing seawater or fresh water contained in a stainless steel, circular double-walled pan which was placed in a cold storage freezer locker operating at −4°F. The double-wall design feature was incorporated to ensure the formation of an ice slab which would freeze uniformly from the top surface down. (During the freezing process, heated air was recirculated through the pan by means of a blower.) Periodic measurements of the slab thickness confirmed that this procedure produced satisfactory results. The subzero test slab was manufactured in an identical manner with the exception that it was frozen in a commercial cold storage plant operating at −30°F.

Typical test specimens exhibited top and bottom surfaces which were both flat and parallel. The top surface of a typical warm sea ice (+17°F) test slab was significantly harder and more solidified than the bottom surface which, as a result of the much higher salinity in the lower layer of the slab, had a tendency to be mushy. However, the subzero sea ice (−13°F) was completely solidified on both top and bottom layers and evidenced a surface hardness appreciably greater than that of the warm ice test specimens.

The salinity content of the seawater as received was 30 ppm. Because of the qualitative nature of these experiments, a precise determination of the salinity profile through the thickness of each ice slab was not obtained. However, the results of two analyses on full core samples by titration for total halide content (Mohr procedure) yielded average salinity contents for the warm ice test specimens of 13 and 19 ppm. For the subzero sea ice slab, a cored sample which was partitioned into three sections through the slab thickness yielded salinity contents of 6.15, 6.22, and 7.61 ppm for the top 50%, middle 38%, and bottom 12%, respectively.

The basic equipment of the test facility (see Fig. 2) consisted of a relatively large circular tank, guide rails, a projectile mass, and various penetrators. The tank was a commercially available portable wading pool, 8 ft in diameter and 20 in. deep. Eight hundred gallons of Pacific Ocean seawater were used to fill the pool. Initially, the tank water was maintained at room temperature; however, in an effort to make the test conditions more typical of the Arctic, the tank water in later tests was cooled to +29°F.

The projectile mass comprised two side plates of stainless steel and a middle plate of brass. Four roller bearings were mounted on the side plates' edges to assist free

sliding motion in the guide rails. The various penetrators which could be screwed into the base of the projectile mass were made of aluminum. Figure 3 shows the projectile mass and penetrators.

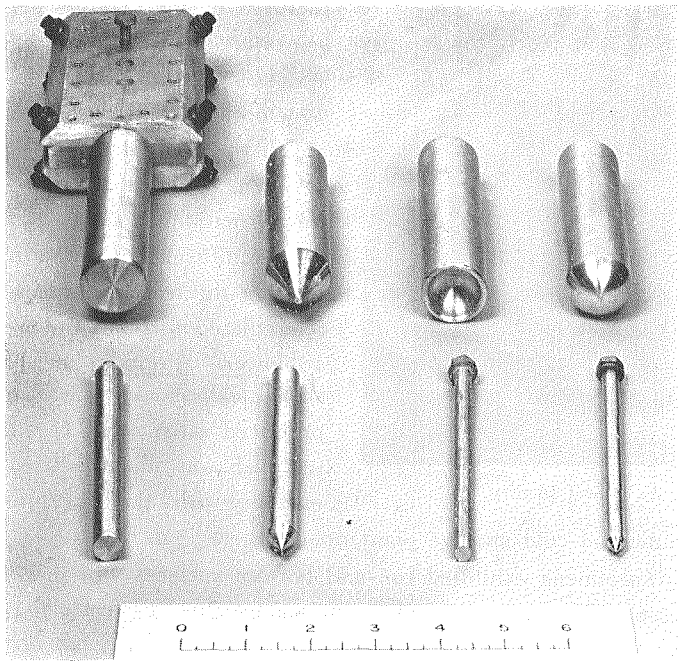

Fig. 3. Projectile mass and various penetrators (scale in inches)

The test procedure and set-up were essentially similar for all experiments. The test slab was removed from the double-walled pan by submerging this unit in the tank of water and allowing the buoyant forces to float the slab free from the pan. The floating test slab was then centrally positioned under the guide rails that contained the projectile mass and its various penetrators. The projectile was released from a selected height and allowed to impact the floating test slab. The penetration process was observed, and the results of perforation and the type of failure were recorded together with the following data: mass of the projectile including penetrator, diameter and profile shape of the penetrator, free-fall height, thickness of the test slab, and temperature and specific gravity of the water in the tank. In addition, by means of embedded thermocouples, the temperature at the center as well as temperatures at midthickness, along a diameter, were obtained for the ice slabs.

III. Test Results

Although impact-penetration experiments were conducted with fresh-water ice and subzero sea ice slabs, only qualitative observations of the penetration process were recorded for these tests.

The quantitative results obtained from experiments on warm sea ice slabs are shown in Figs. 4 and 5, respectively. The ordinates indicate the available potential energy (free fall) while the abscissae represent a characteristic geometric quantity containing the penetrator diameter and the slab thickness. These coordinates were suggested by theory. Figure 4, in particular, portrays the results of tests in which different diameter penetrators having blunt end profile shapes were employed. The results of all tests in which impact occurred at normal incidence are summarized in Fig. 5. Included in this figure are the data points from tests with conical, hemispherical, and concave penetrators.

Temperature distribution and its variation with time are shown for a typical sea ice test specimen in Fig. 6. The pertinent data were obtained from a warm ice (+17°F) slab which floated in seawater at room temperature (+59°F).

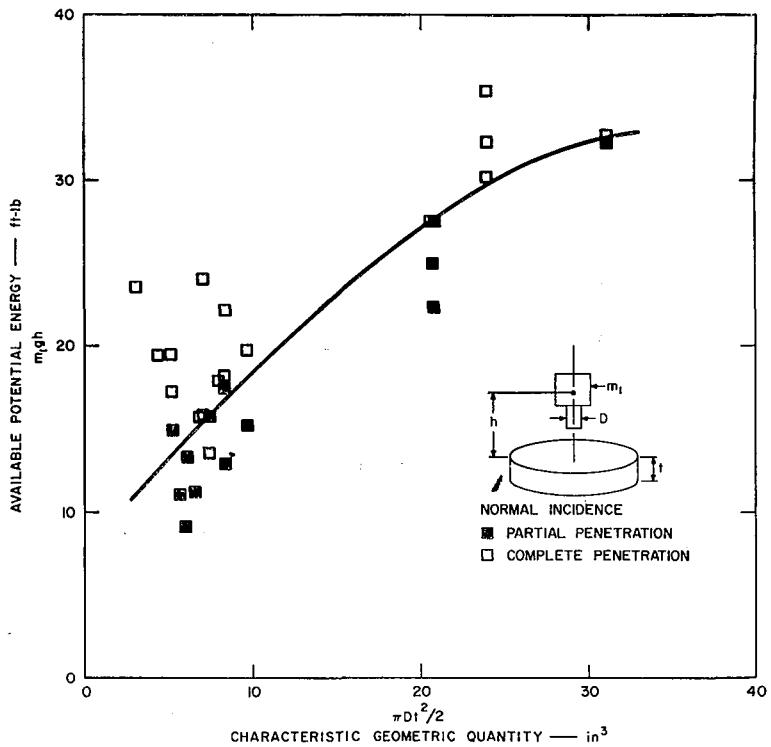

Fig. 4. Plot of test results obtained with blunt end penetrator; warm sea ice (+17°F)

□: Blunt Penetrator

IV. Experimental Observations

Fresh water ice test slabs. Typical fresh water ice test slabs were approximately 3 in. thick. As a consequence of manufacturing the test slabs within the confines of a closed container, the ice showed random surface cracks, along chords, varying from 1/4 to 3/4 in. in depth.

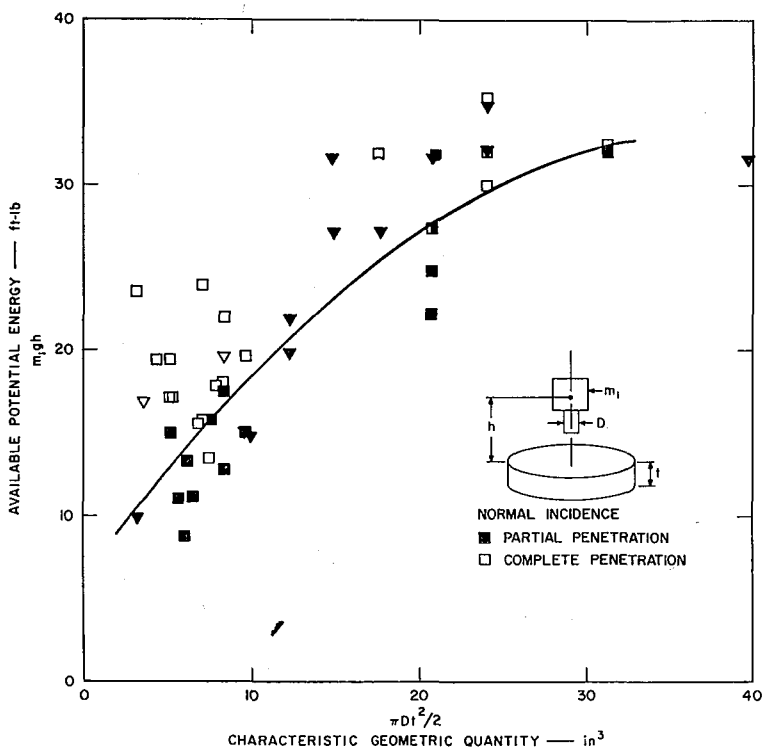

Fig. 5. Plot of test results obtained with conical, hemispherical, concave and blunt end penetrators; warm sea ice (+17°F)

▽: Conical penetrator ⌓: Hemispherical penetrator
⌒: Concave penetrator □: Blunt penetrator

The effects of impact which did not produce complete penetration were restricted to a relatively small volume of ice. In particular, visible local fracture planes issued from the point of contact (conical penetrator) at angles of approximately 45° down from the top surface of the test slab for distances of about 2 in. (see Fig. 7a).

The test slabs which fractured did so by splitting into 3 or 4 pie-shaped segments outlined by radial cracks from the point of impact. The fracture surfaces between adjacent segments were perpendicular to both the top and bottom surfaces of the test slab. In addition, these surfaces were nearly straight in the radial direction (see Fig. 7b) and exceptionally smooth in appearance.

In some tests, impact was made to occur on the surface cracks which were obtained during manufacture. Results indicated that the presence of surface cracks did not contribute to the fracture process. Test slabs which experienced edge impact close to the circular boundary rather than central impact split into two segments (see Fig. 7c).

On the basis of observations only, the conical penetrator was more effective than the blunt penetrator in producing complete fracture of the fresh water ice test slabs.

Sea ice test slabs. The majority of tests were performed using test slabs of frozen seawater at approximate temperatures of +17°F. As a result of making the ice slabs in

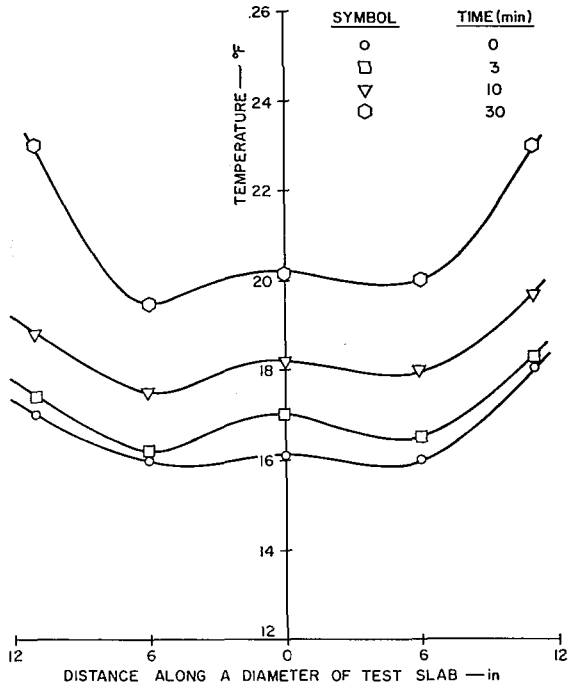

Fig. 6. Typical temperature profiles; warm sea ice (+17°F)

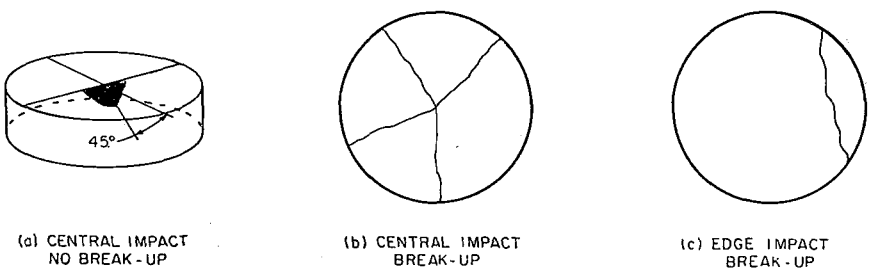

Fig. 7. Views of test slab after impact with $1^1/_4$ in. diameter conical penetrator; fresh-water ice

a closed container, the average salinity values, as well as the salinity distribution profiles through the slab thickness, proved to be an unrealistic representation of typical arctic sea ice. In particular, an accumulation of high salinity layers in the bottom portions of the test slab yielded average salinities that were higher than corresponding values for arctic ice. For these reasons, a complete generalization of the present test results was not possible.

The initial tests, conducted with both conical and blunt end penetrators, indicated that the visible effects of impact were confined to the immediate area of penetrator contact. In cases where perforation did not occur, partial penetration was accompanied by plastic deformation of the adjacent ice. In many instances, partial entry of the

penetrator into the top surface of the ice slab resulted in bulging of the bottom surface along the central axis of impact. A typical cross-sectional view of the ice slab (conical penetrator) showed that a small volume of the material had undergone substantial plastic deformation delineated by a well-defined yield surface, as sketched in Fig. 8.

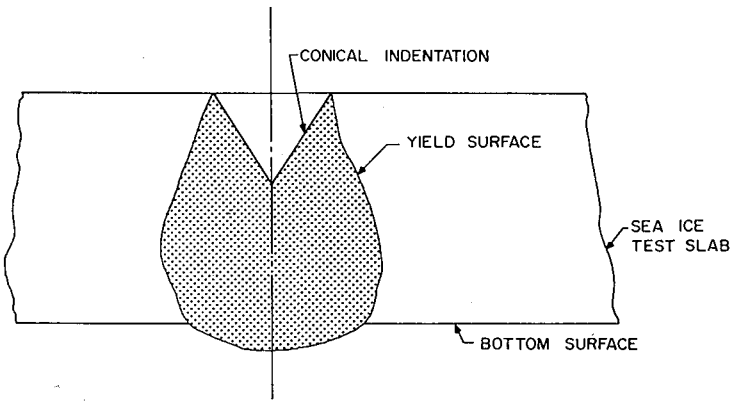

Fig. 8. View of cross-section after impact with $1^1/_4$ in. diameter conical penetrator; warm sea ice (+17°F)

Impact of the penetrator on the sea ice test slabs did not produce surface cracks or fissures, nor fracture along cleavage planes. For every instance in which perforation occurred, a cylindrical plug was sheared out of the ice slab. After ejection of the shear plug, the resulting hole in the ice slab was clean and circular at the top surface, and somewhat enlarged in diameter at the bottom surface. Even at the outer boundary of the ice, where the breaking off of edge sections might have been expected, a shear plug was ejected.

The results from all tests established the superiority of the blunt end penetrator over the conical penetrator. Specifically, for identical test conditions, impact of the conical penetrator produced limited penetration, with two exceptions, while the blunt penetrator perforated the ice readily. The shear plug mode of penetration suggested the use of different penetrator profiles. As a consequence, tests were made with hemispherical and concave penetrators. The relative performance of these penetrators was intermediate between that of the conical penetrator and the blunt penetrator.

In certain tests, it appeared to observers that the passage of the projectile through the test slab was delayed during the perforation process*. The results obtained from these particular tests were used to describe the so-called threshold values of impact velocity for perforation.

Experiments in which the projectile impacted the floating test slab along a path inclined slightly less than 30° to the vertical demonstrated that the conical penetrators, especially the largest diameter one, were incapable of perforating the test slab, being more ineffective in this case than in cases at normal incidence. After impact, the conical penetrator gouged out long troughs in the top surface of the sea ice, and no significant

* Generally, it was observed that the projectile sheared through the slab at impact velocity.

penetration was obtained. The first inclined impact tests with the blunt end penetrator caused the formation of asymmetric craters at the location of impact. However, subsequent tests on thinner test slabs produced both partial penetration and perforation through the mechanisms of shear plug formation.

A series of impact tests was conducted on a subzero sea ice test slab (−13°F) floating in cold sea water (+29°F). Because of limitations on the kinetic energy of the projectile, the ice was not perforated. Instead, on impact, local fragmentation extending to a depth of approximately 1 in. occurred when the largest diameter blunt end penetrator was used and partial penetration resulted with the smallest diameter conical penetrator. These results indicated strongly that the mechanisms of penetration are temperature-dependent.

In all tests performed, the relative scale of projectile, test slab and tank dimensions was such that impact of the falling projectile produced negligible motion of the test slab and virtually no wave motion of the water in the tank. Even in the tests where the ice slab was subjected to inclined impact forces, there was no noticeable horizontal motion of the slab.

V. Mathematical Model and Analysis

For shear plug penetration, a simple mathematical model can be formulated. Based on the classical theory of impact, the equations describing the model behavior are governed by the law of conservation of momentum and the law of conservation of mechanical energy. No account is taken of transient stresses, nor are contact deformations and vibrations of the colliding bodies considered. In agreement with experimental observations, it is assumed that the impact is plastic (no rebound), and that the test slab remains motionless during the shear plug ejection process. Moreover, hydrodynamic drag forces and buoyant body forces on the plug, and sliding friction forces on the penetrator are neglected. Figure 9 shows the model and notation employed.

Conservation of linear momentum yields

$$m_1 v_1 = (m_1 + m_2)\, v_2 \,, \tag{1}$$

where the assumption of plastic impact requires that both masses, m_1 and m_2, travel with the same resulting velocity, v_2, after collision. The free fall velocity of the penetrator mass, m_1, just prior to impact is denoted by v_1.

Conservation of mechanical energy provides a relationship between the amount of kinetic energy imparted to the projectile-plug combination immediately after impact and the amount of work expended in expelling the shear plug from the slab. Since this formulation can only relate initial and terminal velocity states, it is postulated that the plug velocity approaches zero at exit.

Thus,

$$\frac{1}{2}(m_1 + m_2)\, v_2^2 = \int_0^t \tau_{xy}(\eta, \dot{\eta})\, \pi D (t - \eta)\, \mathrm{d}\eta \,, \tag{2}$$

where D is the shear plug diameter, assumed equal to the penetrator diameter, t the

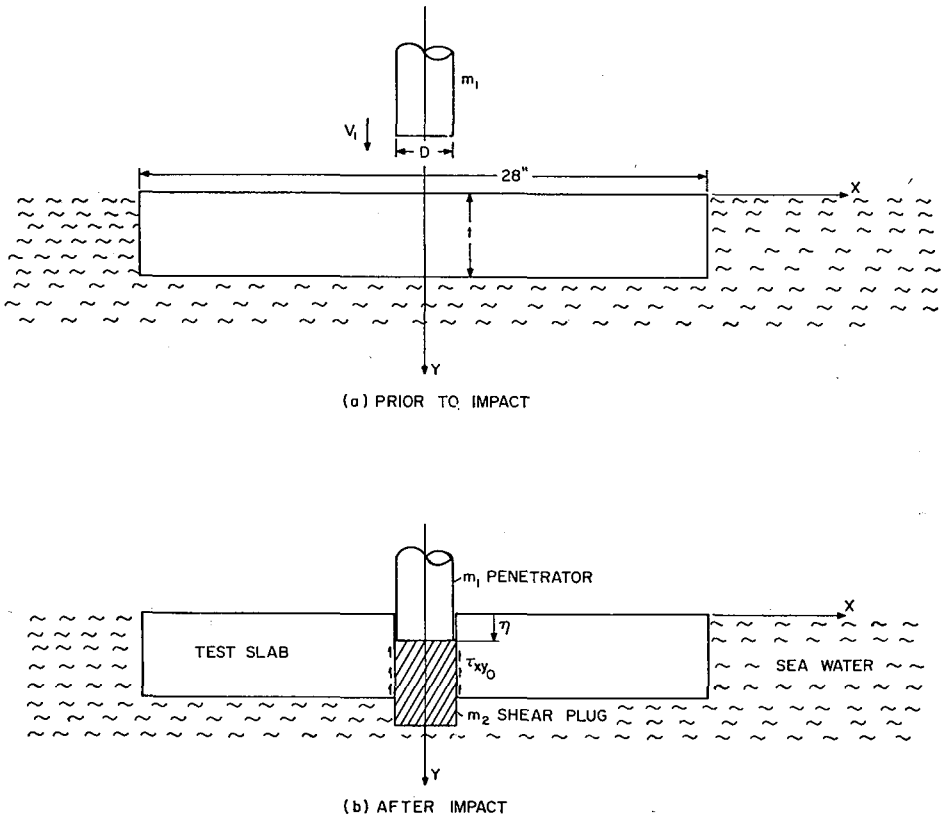

Fig. 9. Sketch of mathematical model for shear plug type of penetration

ice slab thickness, and τ_{xy} the shear yield stress which is in general a function of both position, η, and velocity, $\dot{\eta}$. Substitution of the initial plug velocity, v_2, from eq. (1) into eq. (2) yields

$$\frac{1}{2}\frac{m_1^2 v_1^2}{(m_1+m_2)} = \int_0^t \tau_{xy}(\eta, \dot{\eta})\, \pi D(t-\eta)\, \mathrm{d}\eta \,. \tag{3}$$

Since an experimental determination of the function $\tau_{xy}(\eta, \dot{\eta})$ was beyond the scope of the present investigation, a gross approximation was made to enable an evaluation of the work integral. Thus, the sea ice was assumed to exhibit rigid-plastic behaviour such that ejection of the shear plug occurred at a constant value of shear yield stress, τ_{xy_0}. With this assumption and after performing the indicated integration, there results

$$\frac{1}{2}\frac{m_1^2 v_1^2}{(m_1+m_2)} = \tau_{xy_0}\frac{\pi D t^2}{2} \,. \tag{4}$$

The impact velocity, v_1, due to free fall can be readily expressed in terms of the free-fall height. After rearrangement,

$$\frac{m_1 g h}{\left(1+\dfrac{m_2}{m_1}\right)} = \tau_{xy_0}\frac{\pi D t^2}{2} \,. \tag{5}$$

For the quantities typical of the present experimental program,

$$\frac{m_2}{m_1} \ll 1 , \tag{6}$$

so that

$$m_1 gh \approx \tau_{xy_0} \frac{\pi Dt^2}{2} . \tag{7}$$

Equation (7) relates the available potential energy, $m_1 gh$, to a characteristic geometric term, $\pi Dt^2/2$. These two quantities were used to represent the data obtained from the experiments. It can be seen readily that, if the present shear plug model is valid, a knowledge of the shear yield stress function enables the free-fall height for perforation to be obtained for a given projectile and ice slab.

VI. Discussion of Test Data

An analysis of the simplified mathematical model representing the shear plug mechanism of penetration suggested that various fundamental quantities of the problem comprised two distinct groups. One of these groups, $m_1 gh$, was equivalent to the available potential energy, whereas the other group, $\tau_{xy_0}\ \pi Dt^2/2$, represented the pertinent material and geometric parameters. Since no direct information concerning the shear yield stress, τ_{xy_0}, was obtained during the experiments, it was decided to portray all of the test results on plots with the known quantities $m_1 gh$ and $\pi Dt^2/2$ as ordinates and abscissae, respectively. In this way, characteristic values of τ_{xy_0} were realized from the plotted data.

Figure 4 shows the results obtained with blunt end penetrators. Different values of penetrator diameter, available potential energy, and test slab thickness were employed in these tests. The curve passes through the three threshold data points observed in the experiments, and indicates a smooth, monotonically increasing threshold boundary for perforation. This boundary would be a straight line through the origin if the shear yield stress were equal for all test slabs. With minor exceptions, the impact tests that produced perforation lie above this boundary.

This type of plot furnishes the most significant information obtained from the ice penetration studies. If such a plot is found to be valid for real sea ice, it can be used to predict a projectile's performance. That is, if a projectile of given mass and diameter is released from a particular height, a knowledge of the ice thickness will locate a coordinate position with respect to the threshold boundary. If this point lies above the boundary, perforation will result. In addition, the position of the point with respect to the threshold boundary should provide information concerning the probability of perforation. The threshold boundaries themselves depend on both the mechanism of penetration and typical yield stress values for the ice in question. The former factor appears to be strongly dependent on the characteristic ice temperature while the latter quantities are known to be functions of the ice salinity, brine content, and temperature.

Figure 5 depicts the test results obtained with conical penetrators. Only two projectiles were successful in perforating the sea ice test slabs. Both of these tests employed penetrators of 1/2 in. diameter. In general, relatively greater available potential

energies and thinner test slabs were conducive to perforation at fixed values of penetrator diameter; however, it is interesting to comment on the relative effectiveness of the conical penetrator at different penetrator diameters but nearly equivalent values of available potential energy. Although one test was carried out at a slab thickness of $2^1/_2$ in. while the slab thickness for a different test was $3^1/_4$ in. perforation occurred in the latter case but not in the former. The location of these test results on the plot of Fig. 5 indicates that this behavior is predicted by the theory.

A possible explanation of this phenomenon lies in the difference between the cylindrical-surface areas associated with each penetrator. It is reasonable to assume that the shear yield stress was more or less constant for a given ice slab. Thus, during the perforation process, the resisting force was proportional to area or, more concisely, the penetrator diameter. As a result, a simple calculation shows that for the penetrators employed, $2^1/_2$ times greater resisting force prevailed in the test ($d=1^1/_4$ in.), where perforation did not occur, when compared to the other test ($d=1/2$ in.) which was successful under similar test conditions.

The relative performance of the various penetrator profiles can also be seen in Fig. 5 where the accumulation of data for all impact tests at normal incidence is plotted. Test results obtained at corresponding values of the characteristic geometric quantity, $\pi Dt^2/2$, indicate, on an energy basis, the superiority of the blunt end profile in the perforation process.

The curves drawn in Fig. 6 indicate the temperature profiles along a diameter at midthickness ($y=2$ in.) of a typical test slab. The data for each profile were recorded at given times after placing the ice slab in the tank which contained water at room temperature. Because of this large quantity of water, the slab temperatures increase with time, and at particular values of time the temperatures at points which are closest to the slab's outer edge are noticeably higher than the temperature at the center of the slab. The later temperature was obtained at a point 1 in. above the bottom surface of the slab ($y=3$ in.). This choice of thermocouple location resulted in the slightly higher temperatures at the slab's center.

Finally, it is interesting to examine the experimental points which have been described previously as threshold values. For these data points, simple calculations based on eq. (7) yield respective values for the shear yield stress of 15.8 lb/in^2., 12.5 lb/in.^{2} and 27.5 lb/in.^{2}. These values, when corrected for the high salinity content of the present test slabs, appear reasonable if compared with field data (Zubov, 1945; Paige, 1965).

VII. The Measurement of Resisting Forces During the Perforation Process

In an effort to gain closer understanding of the perforation process, the resisting force-time history experienced by a projectile during its passage through the ice slab was recorded. From this information, it should be possible to obtain a realistic analytical formulation of the critical yield stress function, including strain rate effects, and in turn provide a more exact relationship to describe the perforation process. In addition, for cases where only limited penetration occurs, a history of the impact force delivered to

the slab can be employed as a time varying load input in the determination of transient stresses experienced by the ice.

Resisting force histories were obtained from an oscillographic trace which recorded the output of an Endevco Model 2229 piezoelectric accelerometer mounted in the body of the penetrator. The accelerometer signal was passed through a Kistler Model 504 charge amplifier and a SKL Model 302 Dual Filter, before serving as input to a Model 502 A Tektronix dual beam oscilloscope. The oscilloscope was triggered externally from the output of a contact microswitch tripped by the falling projectile just prior to impact.

Impact velocity was obtained by reading, on an electronic counter, the elapsed time between two consecutive signals furnished during passage of the projectile body's lower and upper edges across the wiper arm of a single microswitch. In this manner, the fixed projectile body length was employed as the interval of distance in the velocity calculation.

Finally, in order to ascertain the moment at which the penetrator's impact end emerged from the ice slab (ice-water interface), a signal was captured by a prepositioned magnetic head from a magnetized pinpoint embedded in the projectile slab's outer side. The relative pickup position was determined by utilizing the measured thickness of the ice slab. This signal was recorded on the second beam of the oscilloscope, and for corresponding time bases readily furnished an appropriate cutoff for identifying the value of resisting force at exit from the ice slab.

Two representative oscillograms taken from initial tests performed with this system are shown in Figs. 10 and 11. Figure 10 portrays the deceleration or resisting force experienced by the projectile with a blunt end penetrator during passage through a 2 in. thick slab of styrofoam. The styrofoam material was used extensively in this investigation since its physical structure and reaction to impact loading correspond with the warm sea ice employed in the previous tests. In addition, the almost uniform properties and homogeniety of this material plus its ease of handling, in large contrast to similar quantities associated with sea ice, are extremely useful in clarifying certain aspects associated with the phenomenon of perforation as opposed to effects due to material properties.

Figure 10 indicates that the resisting force develops an initial linear increase with

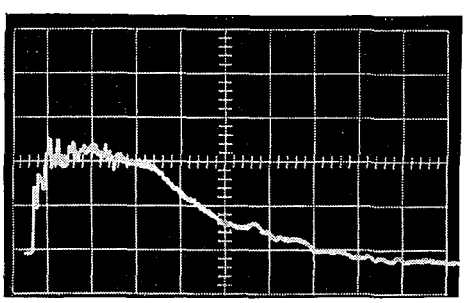

Fig. 10. Resisting force experienced by projectile during perforation of a 2 in. styrofoam slab
Gain : 10 g/cm, Sweep : 2 ms/cm

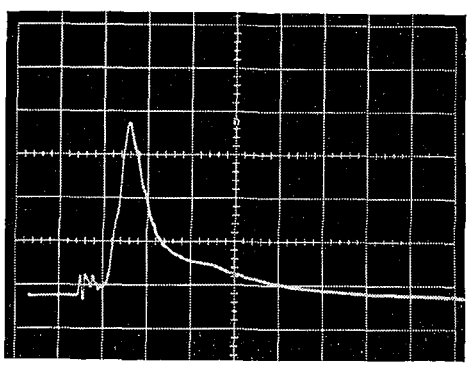

Fig. 11. Resisting force experienced by projectile during perforation of a 3 in. sea ice slab
Gain : 50 g/cm, Sweep : 2 ms/cm

time corresponding to elastic compression of the slab material. When sufficient impact energy is absorbed, the formation of a plug at essentially constant force or, more exactly, constant shear yield stress takes place. After this process in which the material bonds over a cylindrical yield surface are sheared, the continued ejection of the plug occurs with exponentially decreasing resisting force. The lowered values of force experienced by the projectile during this stage are a result of the decreasing contact area during plug ejection and, probably, a reduced value of shear stress, or kinematic friction stress, during ejection.

The styrofoam plugs expelled from the slab showed evidence of having been compressed into the plastic range; whereas, the cylindrical surfaces indicated forceful shearing of the slab material during formation of the plug.

Figure 11 portrays similar information from an impact test on a 3 in. sea ice slab. A resisting force history is noted which suggests linear compression with increasing force up to a well-defined yield point followed immediately by an exponentially decreasing force as the shear plug is ejected from the slab.

The record in this case indicates that the maximum resisting forces to penetration occur immediately after impact, within the topmost layers of the ice slab. This behavior is predicted by theory based upon the crystallographic structure of sea ice where it is known (Pounder, 1965, 20–23) that the orientation and size of the ice crystals are most regular within the surface layer. The attendant mechanical strength of the sea ice is higher in the upper layer and it is to be expected that the greatest resistance to penetration will occur in this region.

VIII. Summary and Conclusions

An experimental program was conducted in which circular ice slabs floating in a tank of seawater were subjected to the impact of a freely falling projectile. Fresh-water ice, seawater ice at +17°F, and seawater ice at −13°F were employed for the test slabs.

A projectile weighing approximately 5 lb was fitted with cylindrical penetrators of different diameters ($^5/_{16}$, $^1/_2$ and $1^1/_4$ in.) and different end profiles (conical, hemispherical, concave and blunt), and allowed to impact the test slab at velocities of 8 to 21 ft/sec.

On the basis of tests performed over the foregoing range of variables, the following results were realized:

The mechanism of perforation depended on whether fresh water ice or sea ice was being investigated. The fresh ice test slabs fractured into large segments along radial cleavage planes whereas sea ice test slabs at +17°F were perforated by the formation of a shear plug.

The mechanism of perforation depended on the characteristic temperature of the ice. For example, it was not possible to perforate the subzero (−13°F) sea ice test slab with the available penetrator mass and drop weight. However, the same penetrator mass, under similar test conditions, readily produced perforation in the warm sea ice (+17°F) test slabs.

The results obtained from a relatively large number of tests on sea ice at +17°F

indicated that shear plug ejection was present in every instance of perforation. The following observations were applicable for this type of behavior:

The conical penetrator was relatively ineffective in perforating the test slab; however, the blunt end penetrator performed satisfactorily. Performances of both the hemispherical and concave penetrators were intermediate to the conical-blunt extremes. For a given penetrator and ice slab, a minimum or threshold value of available kinetic energy at impact was required to produce perforation. This energy appeared to be related to the shear yield stress of the ice, the square of the thickness of the test slab, and the diameter of the penetrator.

Tests were also conducted in which the projectile was made to impact a sea ice test slab at approximately 30° incline to the vertical direction. Qualitative results were similar to those obtained at normal incidence. That is, perforation resulted from the ejection of a shear plug; and in this process, the blunt end penetrator was significantly more effective than the conical penetrator.

The author is grateful to the Office of Naval Research and the Naval Ordnance Laboratory (White Oak) for sponsoring the investigation and for permission to publish this paper.

References

1) BENERT, R. 1963 Penetration of shaped charges into frozen ground. *CRREL Tech. Rept.*, **130**.
2) CHAREST, J., DULER, P. and RINEHART, J. 1965 Mechanics of penetration of piles into permafrost. *CRREL Tech. Rept.*, **122**, 1–98.
3) KINGERY, W. D. 1963 Ice and Snow, M.I.T. Press, Cambridge, Mass., 684 pp.
4) PAIGE, R. 1965 Personal Communication, Polar Division, Naval Civil Engineering Laboratory, Port Hueneme, California.
5) POUNDER, E. R. and LITTLE, E. M. 1959 Some physical properties of sea ice. I. *Canad. J. Phys.*, **37**, 443–451.
6) POUNDER, E. R. 1965 The Physics of Ice, Pergamon Press, London.
7) WILSON, D. P. 1964 The Arctic, a Selective Bibliography, *NSL Tech. Memo., No.* **904**, 3-03-64.
8) ZUBOV, N. N. 1945 L'dy Arktiki (Arctic Ice), Glavesmorputi, Moscow, 360 pp.

Appendix

A large amount of work and some significant results have been obtained since submission of the original paper. This appendix attempts to summarize these findings and presents the important features of a new theory for predicting the impact velocity necessary to perforate a sea ice slab.

In retrospect, the previous results showed that sea ice slabs manufactured in a closed container contained relatively large amounts of brine and had high salinity contents (warm sea ice +17°F), and that sea ice in this condition was perforated invariably by the expulsion of a cylindrical shear plug when impacted by a blunt end cylindrical penetrator. This behavior was qualified in generality by the unrealistic physical composition of the sea ice test slabs. In order to avoid these difficulties, a new means was devised for the manufacture of sea ice which resulted in significantly lower salinity contents for the test slabs. Impact tests performed on these slabs indicated a different perforation mechanism which has been classified as a type of failure resulting in the formation of a cylindrical-conical shear plug. On the basis of this model, a new analysis was developed to predict perforation impact velocity.

The theoretical predictions compare favorably with experimental results obtained from both styrofoam and sea ice test slabs. At present, the range of variables which has been explored is narrow and efforts are currently underway to expand considerably the scope of the experiments. To this end, a rifle-powered projectile assembly capable of producing impact velocities up to 500 ft/sec (1 lb projectile) is now in operation.

Test Equipment and Procedure

In lieu of a shallow closed container, an insulated commercial oil drum containing seawater was placed in the freezer room (see Fig. A 1); the sea ice was then formed unidirectionally from the top surface. The drum, which was mounted on a dolly to facilitate positioning under the guide rails, was wrapped by heating tape whose output was controlled by a series Powerstat. With this setup, the rate of freezing and resulting ice slab thickness could be adjusted; however, during actual data runs the system was inoperative to avoid interfering with the natural growth process of the sea ice. The inner circumference of the drum was lined by a 1 in. thick waterproof neoprene rubber pad to a depth of 8 in. This allowed the sea ice slab to form under very much lower radial stresses than would be present within the confines of the "rigid" drum wall. As a result, ice surface cracks, fissures, and humping were eliminated completely. Finally, a relief valve was provided at the bottom of the drum to enable the release of accumulated hydrostatic

Fig. A 1. Oil drum and frozen sea ice slab in freezer

pressure during the ice formation process.

The ratio of typical ice thickness to underlying seawater depth was approximately 1 : 7. Characteristic salinities obtained for the ice produced in this "semi-closed" system ranged from 7 to 13 ppm, considerably lower than those typical of the previous study. Furthermore, in the present study, more accurate temperature profiles were recorded by using an array of 10 thermocouples spaced vertically at $^1/_2$ in. intervals. In contrast to the previous work, all tests were performed "in-place" in the cold room, thereby eliminating handling and soaking of the ice slabs' top surfaces' with seawater.

To obtain high impact velocities, a rifle-powered projectile system was assembled. This included a 458-Winchester Magnum, "smooth-bore" rifle which can propel a projectile having various interchangeable penetrator heads (see Fig. A 2) at velocities of 50 to 500 ft/sec. Two sets of foil screens, 6 in. apart, were employed individually in a "make" electronic circuit to trigger a counter that indicated the actual impact velocities.

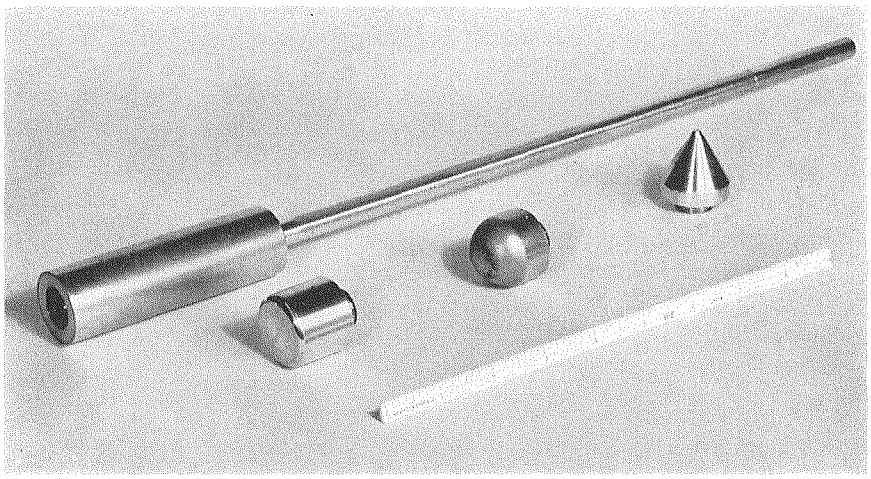

Fig. A 2. Rifle propelled penetrator and various end profiles

Analysis

Because the previous test series demonstrated the superiority of the blunt end penetrator over the conical penetrator in perforating sea ice, all tests are being carried out presently using the blunt profile. Test results have indicated that, in a corresponding range of the ratio, ice thickness to penetrator diameter, the mechanism of perforation observed for the lower salinity sea ice of the present study was significantly different from the cylindrical shear plug behavior observed before. For example, perforation resulted in the formation of the cylindrical-conical shear plug depicted schematically in Fig. A 3 and shown actually, in external cross section, for a 2 in. thick styrofoam slab in Fig. A 4. As a result of these observations, a new analysis was developed.

It is conjectured that, on impact, the high stress concentration around the perimeter AB of the blunt penetrator (Sneddon, 1951, pp 462–468) causes local yielding due to shear. This results in the well-defined cylindrical shear-yield surface AA′–BB′ when the penetrator undergoes a vertical displacement, ξ. Further penetration compresses a cylindrical vol-

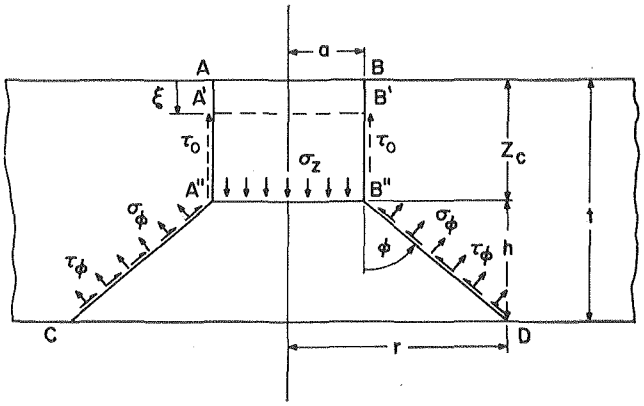

Fig. A 3. Schematic drawing of cylindrical-conical plug model

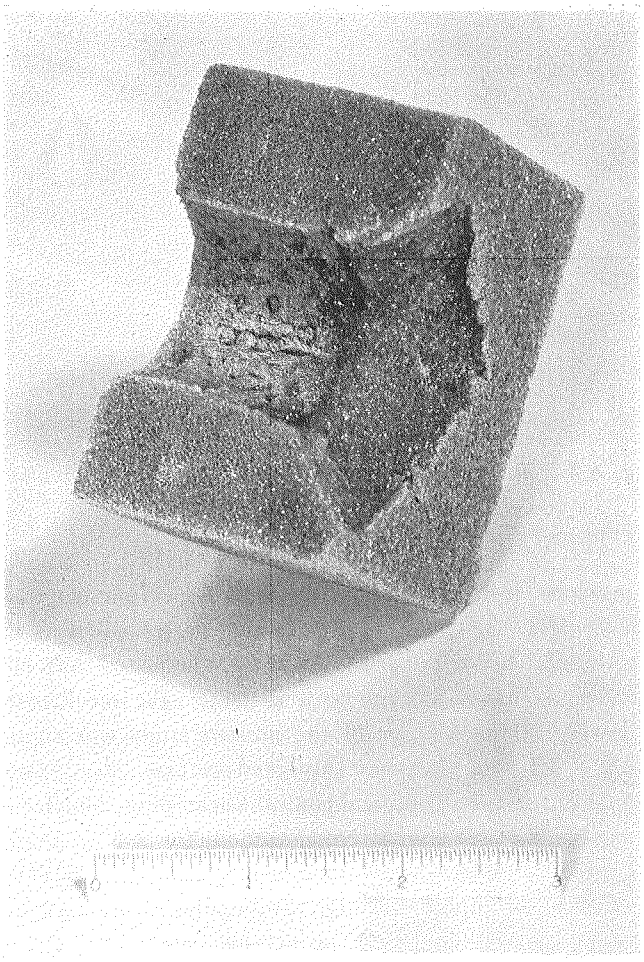

Fig. A 4. Photograph of profile obtained in the perforation of a 2 in. styrofoam slab by a blunt end penetrator

ume of material under the penetrator along the path AA″–BB″. During this process, the material being compressed absorbs kinetic energy of the projectile both in overcoming the surface traction due to the shear yield stress, τ_0, and the resisting forces due to compressive normal stresses, σ_z. It is postulated further that these latter stresses obey a spring-law relationship; that is, they increase linearly with vertical displacement, ξ. Eventually, continued compression of the sheared-out, cylindrical plug results in a normal force, $\sigma_z \pi a^2$, where a is the penetrator radius, large enough to tear the conical frustum of material A″B″ CD out of the slab. This event occurs when the tensile rupture stress of the slab material, σ_φ, is overcome on the surface A″C–B″D. Once the plug has been formed, a certain amount of elastic recovery occurs such that the cylindrical plug expands back along the path A″A′–B″B′ to an intermediate position. Thus, the resulting plug produced in perforation of the slab by a cylindrical, blunt end penetrator is cylindrical-conical in shape.

The present theory attempts to formulate mathematically a means for predicting the impact velocity necessary to perforate a slab for which the resulting failure mechanism is characterized by the formation of a cylindrical-conical plug. The theory considers that under the relatively short time intervals associated with impact loading, the material behaves elastically up to yielding or fracture, both on loading and unloading. Since the phenomenon of spalling has not been observed in any tests, the present analysis does not include stress wave effects but relies on rigid body dynamics in its formulation. Furthermore, at incipient failure, the motion of the conical frustum plug with respect to the underlying seawater is negligible; therefore, hydrodynamic forces are neglected.

Reference is made to Fig. A 3. Equilibrium equations for the plug in the radial and vertical directions can be written as follows*:

r direction $$\sigma_\varphi A \cos\varphi - \tau_\varphi A \sin\varphi = 0\,, \tag{A 1}$$

z direction $$\sigma_z \pi a^2 - \sigma_\varphi A \sin\varphi - \tau_\varphi A \cos\varphi = \rho V \frac{\mathrm{d}^2\xi}{\mathrm{d}t^2}\,, \tag{A 2}$$

where $$A = \pi(r+a)\sqrt{h^2+(r-a)^2}\,. \tag{A 3}$$

---

* a radius of penetrator
h, r base height and radius of conical frustum plug, respectively
k dynamic compression modulus relating compressive stress and penetrator displacement
m_1, m_2 mass of penetrator and plug, respectively
t thickness of slab
v_1, v_2 impact and exit velocity of penetrator, respectively
v_c critical impact velocity
z_c critical displacement of penetrator at incipient failure
η dimensionless ratio
ξ instantaneous displacement of penetrator
φ vertex angle of conical frustum plug
ρ "locked" mass density of material in conical frustum
σ_z compressive bearing stress resisting penetration
σ_φ tensile rupture stress acting normal to conical surface
τ_φ shear stress acting parallel to conical surface at fracture
τ_0 cylindrical shear yield stress resisting penetration
$\bar{F}(\varphi, \eta)$ minimum value of $F(\varphi, \eta)$ with respect to φ, η fixed
V volume of material in conical frustum

The radial equilibrium equation is not exact since it implies that the net radial force acting on the conical surface is zero. However, the equations of equilibrium are written for a rigid plug and because in the vertical direction only one-dimensional motion is considered, it is assumed that on the slant surface area of the plug the reaction forces needed for equilibrium are vertical and the complementary horizontal radial forces are identically zero. For an elastic plug, contact surface deformations of the plug and slab due to surface tractions must be obtained and an equation expressing compatibility of deformations employed to relate, mutually, the contact surface stresses, σ_φ and τ_φ. This problem would be exceptionally difficult to solve and its consideration was not warranted in this investigation. —Combining eqs. A 1, A 2 and A 3 yields*

$$\sigma_z \eta^2 = \sigma_\varphi \frac{(\tan\varphi + 2\eta)(\tan^2\varphi + 1)}{\tan\varphi}, \qquad \text{A 4}$$

where

$$\eta = \frac{a}{t - z_c}.$$

Next, the conservation of mechanical energy is used to relate the available kinetic energy at impact to the work done in expelling the cylindrical-conical plug. Thus, for negligible exit velocity

$$\frac{1}{2} m_1 v_1^2 = \int_0^{z_c} \tau_0 2\pi a (z_c - \xi)\, \mathrm{d}\xi + \int_0^{z_c} \sigma_z \pi a^2\, \mathrm{d}\xi, \qquad \text{A 5}$$

where the dynamic compressive stress, σ_z, is assumed to vary linearly with displacement, ξ, according to

$$\sigma_z = k\xi. \qquad \text{A 6}$$

Elastic recovery has been neglected since pertinent accurate experimental data were not obtained. However, observations indicated that as much as 20% recovery could occur. (This phenomenon will result in lower critical impact velocities than those predicted by eq. A 5.) After integration and rearrangement, eqs. A 5 and A 6 yield

$$z_c = \sqrt{\frac{m_1 v_1^2}{\pi a [2\tau_0 + ak]}}. \qquad \text{A 7}$$

Substituting $\sigma_z = k z_c$ in eq. A 4, there results

$$z_c = \frac{\sigma_\varphi}{k} F(\varphi, \eta), \qquad \text{A 8}$$

where

$$F(\varphi, \eta) = \frac{(\tan\varphi + 2\eta)(\tan^2\varphi + 1)}{\eta^2 \tan\varphi}. \qquad \text{A 9}$$

The *critical* impact velocity is obtained when incipient failure occurs at the *minimum* possible equilibrium value of σ_z. From eq. A 4, this condition is met when $F(\varphi, \eta)$ is a minimum. Finally, the critical impact energy is given by

$$\frac{1}{2} m_1 v_1^2 = \frac{\pi a^4}{2} k \sigma_\varphi^{*2} [1 + 2\tau_0^*] \bar{F}^2(\varphi, \eta), \qquad \text{A 10}$$

* The inertia forces in eq. A 2 have been neglected since the mass of the plug is extremely small when compared to the mass of the penetrator and it follows that the inertia force is also small when compared to the contact force, $\sigma_z \pi a^2$.

where

$$\sigma_\varphi^* = \frac{\sigma_\varphi}{ak} \qquad \tau_0^* = \frac{\tau_0}{ak} ,$$

and

$$\bar{F}(\varphi, \eta) = F(\varphi, \eta) ,$$

when

$$\left.\frac{\partial F}{\partial \varphi}\right|_\eta = 0 .$$

A plot of $F(\varphi, \eta)$ as a function of φ, together with a locus through the minima, $\bar{F}(\varphi, \eta)$, is shown in Fig. A 5. To obtain the critical impact velocity for a particular slab, the following calculations are required. Given: t, a, m_1, τ_0, k, σ_φ. A value of v_1 is assumed such that the quantity z_c given by eq. A 7 satisfies the relationship $0 \leq z_c \leq t$. Then, the value of z_c obtained from eq. A 8 is reconciled to the first calculated value of z_c by a cut-and-try process such that the simultaneous equations are mutually satisfied. The value of v_1 thus realized, satisfies eq. A 10 and is the critical impact velocity.

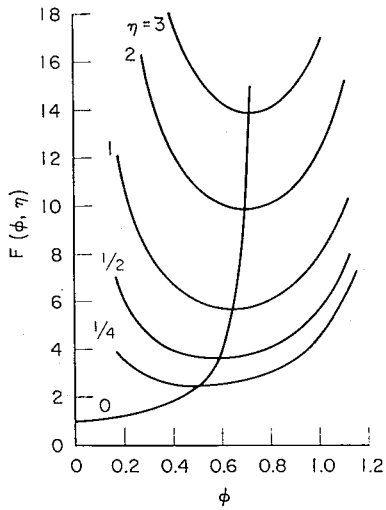

Fig. A 5. Plot of $F(\varphi, \eta)$ vs. φ for various values of η

Test Results

The experimental results obtained from tests on both sea ice and styrofoam are shown in Figs. A 6 to A 8, inclusive. In addition, the predictions of the present theory for the slabs tested are also included. For styrofoam, the static material properties furnished by the manufacturer were employed for the quantities: τ_0, σ_φ and k. How-

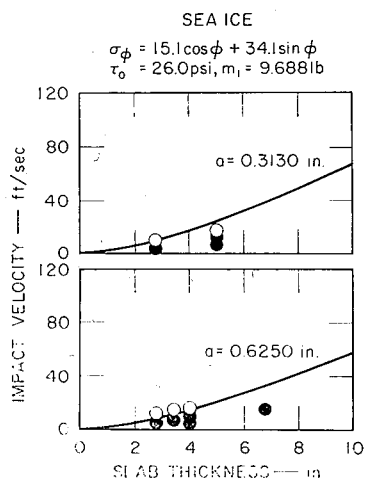

Fig. A 6. Plot of critical impact velocity vs. slab thickness for sea ice; cylindrical blunt end penetrator

● No perforation
○ Perforation

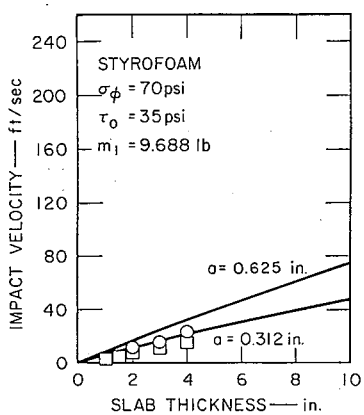

Fig. A 7. Plot of critical impact velocity vs. slab thickness for styrofoam; cylindrical blunt end penetrator

○ a=0.625 in. □ a=0.312 in.

ever, for the sea ice test slabs, a different scheme was employed. Recent results published by Dykins (1966) give tensile strength data for sea ice grown in a confined system. Dykins reports two significant tensile strengths, one in the vertical direction, one in the horizontal direction. In the present work, these individual strengths were combined as component stresses to yield a resultant tensile rupture stress, perpendicular to the conical surface, as a function of the cone angle, φ. Furthermore, the values obtained by Dykins were for sea ice slabs at $-10°C$ and approximately 7 ppm salinity. These values were individually corrected to yield values appropriate to the present experiments ($-7°C$ and $7\sim13$ ppm) by employing the results of Assur (1958) concerning the relative tensile strength of sea ice as a function of temperature and salinity.

The shear yield strength was assumed to equal 1/2 the tensile strength, this choice corresponding to the Tresca yield conditions for unidirectional principle stress. Finally, the dynamic compression modulus, k, was obtained from the oscillographic record showing the resisting force-time history (see Fig. 10) by measuring the slope of the initial linear deceleration curve.

Figures A 6 and A 7 show the critical impact velocity, v_1, plotted against slab thickness, t. Experimental data points are represented by circles and squares while the appropriate theoretical threshold boundaries for perforation are given by the solid curves. Each data point represents the average result of many tests; blackened data points refer to tests in which perforation did not occur, the opposite was true for blank data points.

In Fig. A 7, the circles and squares represent tests with $1^1/_4$ and $^5/_8$ in. diameter blunt end penetrators, respectively. The agreement between theory and experiment appears satisfactory over the limited range of test variables. Figure A 8 shows the average penetration depth, z_c, during which shear yielding occurred, as a function of slab thickness for tests in which perforation did occur. The depth z_c was not measured readily in tests on sea ice and so this information is only given for the styrofoam test slabs. The trend of the data obtained experimentally agrees with theoretical predictions.

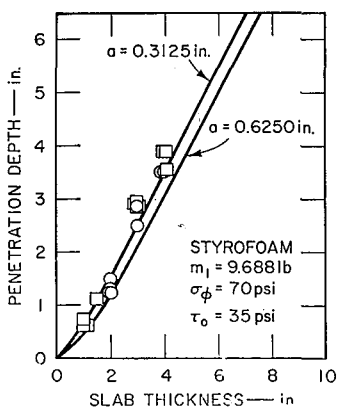

Fig. A 8. Plot of z_c vs. slab thickness for styrofoam; cylindrical blunt end penetrator

○ a=0.625 in. □ a=0.312 in.

On the basis of extensive tests on styrofoam, and selected tests on sea ice, it seems apparent that the behavior of sea ice slabs can be broadly categorized on the basis of an aspect ratio relating slab thickness to penetrator diameter. These observations are summarized in Fig. A 9 which is largely self-explanatory. The present theory covers the range of t/D from 1.5 to 3. At values of t/D less than 1.5, fracture due to tensile hoop stresses occurs. Impact problems of this type can be analyzed by thin plate or thick plate theory; in particular, thin plate problems are discussed by Goldsmith (1960). At greater t/D ratios, an ogival plug is obtained; thus, strictly speaking, the present theory is inapplicable in this case. However, when the cylindrical-conical plugs obtained in the present experiments are cut across a vertical, diametrical

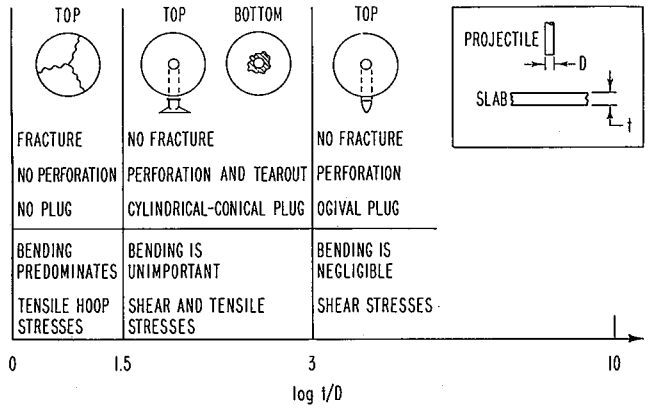

Fig. A 9. Mechanisms of perforation observed in experiments on sea ice and styrofoam as a function of slab thickness to penetrator diameter ratio

plane, the outline of an ogival yield surface within the plug is strongly apparent. Thus, in addition to the "rigid-body" formation of a "cylinder-cone" plug, an interior deformation process in which plastic behavior is evidenced also occurs during the perforation process. The ogival yield volume corresponds in appearance to the slip-line field at the yield point for the indenting of a finite width slab by a flat width die, Hill (1960). Further work is being pursued in this area at present.

Future effort in this problem will include a large experimental program to investigate the perforation behavior of sea ice at, or beyond, the second eutectic temperature of −23°C. It is expected that considerably higher impact velocities will be required to perforate this relatively stronger ice. In addition, the reduced brine volume and salinity content characteristic of subzero sea ice can possibly result in significantly different mechanisms of perforation for which the present theory might be inapplicable. This information should be available in the near future, since field tests at Point Barrow, Alaska, will be conducted this winter.

References

1) ASSUR, A. 1958 Composition of sea ice and its tensile strength. *In* Arctic Sea Ice, *Nat. Acad. Sci. -Nat. Res. Council U.S.A., Publ.* **598**, 106–138.
2) DYKINS, J. E. 1966 Tensile and creep strength data for sea ice grown in a confined system. NCEL, Port Hueneme, California.
3) GOLDSMITH, W. 1960 Impact, Edward Arnold Ltd., England.
4) HILL, R. 1950 The Mathematical Theory of Plasticity, Oxford Press, England, 356 pp.
5) SNEDDON, I. 1951 Fourier Transforms, McGraw Hill Inc., New York.